Appl. Phys. B 82, 449–453 (2006)
DOI: 10.1007/s00340-005-2073-1

Applied Physics B
Lasers and Optics

N.W. PU[1,✉]
T.C. LI[2]

Pulse-echo measurement of longitudinal sound velocity in nanometer thin films

[1] Department of Applied Physics, Chung Cheng Institute of Technology, National Defense University, Tahsi, Taoyuan 335, Taiwan R.O.C.
[2] School of Defense Science, Chung Cheng Institute of Technology, National Defense University, Tahsi, Taoyuan 335, Taiwan R.O.C.

Received: 15 August 2005/Revised version: 20 October 2005
Published online: 8 December 2005 • **© Springer-Verlag 2005**

ABSTRACT We propose a method to measure the longitudinal sound velocity in thin films of a few nanometer thickness using laser-based picosecond ultrasonics. In periodic multilayer structures, picosecond pulse-echo techniques were used to measure the effective sound velocity, which is related to the velocities of individual constituents through the superlattice phonon dispersion relation. The individual sound velocities can then be extracted, provided two or more effective velocities are obtained from multilayers of different thickness ratios. Longitudinal sound velocities in ion-beam sputtered Mo and amorphous Si films of 2 to 5 nm thickness have been determined to be 98 and 94% of the bulk speed, respectively. We believe this technique has general applicability to sound velocity measurement in ultra-thin films.

PACS 68.60.Bs; 68.65.Ac; 78.47.+p

1 Introduction

There is an ever-increasing demand for measuring the velocity of sound in thin films of ever-decreasing thickness. For example, design of Bragg reflectors in acoustic wave resonators or filters requires knowledge of accurate longitudinal acoustic velocities of materials in thin films. Moreover, important elastic properties such as stiffness constants and Young's modulus of thin films are often derived from sound velocity measurement. The conventional ultrasonic pulse-echo technique for measuring sound velocity is not applicable to films due to its low time resolution. Brillouin scattering can be used to measure the longitudinal and Rayleigh sound velocities indirectly. Another indirect method measures the shift of a substrate resonant frequency caused by the deposited film. The substrate can be a reed [1] or a piezoelectric crystal [2, 3]. However, its application is limited to films of thickness $\geq 1\ \mu$m.

The direct pulse-echo measurement of sound velocity re-attracted attention when the picosecond ultrasonic technique was first introduced in 1986 by Thomsen and coworkers [4]. This technique employs an ultrafast mode-locked laser for generation and detection of ultrashort acoustic pulses in a pump-probe configuration. Acoustic pulses with frequencies up to hundreds of GHz are photoexcited with pump laser pulses, and detected by monitoring the reflectance of a time-delayed probe beam. Measurements on transparent films can be made by adding an ultra-thin light-absorbing transducer film. In general, temporal resolution of a few picoseconds can be achieved. This technique is unique in that it permits a measurement of the longitudinal sound velocity, along the growth direction, which is difficult to explore by other means. It has been widely applied to many opaque and transparent films [4–12], and has proven to be a very powerful tool for thin-film characterization.

To avoid overlapping of successive echo signals, the round-trip time must be longer than the acoustic pulse width. This sets a lower limit on the film thickness that can be measured directly by picosecond ultrasonics. The minimum thickness of a film that has been measured is ~ 20 nm [10]. However, in most cases significant distortion and interference due to overlapping can occur for thickness below 50 nm. Besides, given a fixed temporal resolution, the uncertainty in sound velocity increases as film thickness is reduced. Therefore, it is hard to extend the application of this technique to thinner films. In this paper, we propose a novel approach to measure the longitudinal sound velocity in thin films of less than 7 nm thickness with picosecond ultrasonics. By stacking bilayers of two different materials, a multilayer can be made thick enough for a high-accuracy measurement of the acoustic time of flight. It should be noted that the acoustic pulse propagates freely without reflection or scattering at interfaces in a perfectly periodic structure according to Bloch's theorem. Therefore, the pulse-echo technique works the same way as it does in a homogeneous film, except that it yields an effective superlattice sound velocity in this case. The effective sound velocity is related to the velocities of individual constituents through the superlattice phonon dispersion relation [13]. If two or more samples with multilayers of different thickness ratios are measured, the individual sound velocities of the two films can be determined, as will be shown in Sect. 2.

2 Acoustic phonons in periodic multilayers

Brillouin scattering has been used for velocity measurements in many superlattices such as Nb/Cu [14],

✉ Fax: +886-3-390-0483, E-mail: nwpu@ccit.edu.tw

Mo/Ni [15], V/Ni [16], Au/Cr [17], and SnTe/Sb [18]. Interesting elastic anomalies were observed in these systems. This technique however, is limited to the study of surface (Rayleigh) acoustic waves in these opaque films. It is a great advantage of the picosecond ultrasonic technique to allow investigation of bulk acoustic waves, even in opaque materials.

In a superlattice or a periodic multilayer, the artificial periodicity significantly modifies the behaviors of acoustic phonons. The phonon dispersion curve is folded back into a series of minibranches, and gaps open at the boundaries and in the center of the mini-Brillouin zone [19, 20], of dimension $2\pi/d$, where d is the modulation period. These gaps are induced by the difference in acoustic properties of the two constituents. The wave number q becomes complex in the frequency gaps. No propagating modes are allowed within these gaps.

Consider a superlattice structure made up of alternating layers of thicknesses d_1 and d_2 , densities ϱ_1 and ϱ_2, and longitudinal sound velocities c_1 and c_2 (along the growth direction). The repeat distance d equals $d_1 + d_2$. Since the laser spot size is much greater than the film thickness, the problem is reduced to a one-dimensional one with the equation of elasticity:

$$\varrho(z)\frac{\partial^2 u(z,t)}{\partial t^2} = \frac{\partial\sigma(z,t)}{\partial z}\,, \tag{1}$$

where u is the displacement in the z direction, and σ is the zz component of the elastic stress tensor, which is related to u by

$$\sigma(z,t) = C_{33}(z)\frac{\partial u(z,t)}{\partial z} = C_{33}(z)\eta(z,t)\,. \tag{2}$$

$\eta = \partial u/\partial z$ is the zz component of the elastic strain tensor, and $C_{33} = \varrho c^2$ is the corresponding stiffness constant. The values of C_{33}, c and ϱ depend on the particular layer. The normal mode solutions are Bloch waves, which can be obtained by solving (1) and (2) along with the boundary conditions that u and σ are continuous at each interface. The superlattice phonon dispersion relation for these Bloch waves is given by [13]:

$$\cos(qd) = \cos(\omega d_1/c_1)\cos(\omega d_2/c_2) - \frac{1}{2}\left(\frac{Z_1}{Z_2}+\frac{Z_2}{Z_1}\right)\sin(\omega d_1/c_1)\sin(\omega d_2/c_2)\,, \tag{3}$$

where $\omega = 2\pi\nu$ is the angular frequency of the phonon mode, and $Z_i = \varrho_i c_i$ ($i = 1$ for Si; 2 for Mo) are the acoustic impedances for the two materials. Figure 1a and b display two examples of calculated longitudinal acoustic (LA) phonon dispersion for Si/Mo multilayers with relative Mo thickness ratios $\Gamma(\equiv \frac{d_2}{d}) = 0.4$ and 0.6, respectively. The material parameters used for the calculation are assumed to be the bulk values for amorphous Si (a-Si) and Mo: $\varrho_1 = 2.29\ \text{g/cm}^3$ [21], $\varrho_2 = 10.22\ \text{g/cm}^3$ [22], $c_1 = 8.30$ km/s (directionally averaged crystalline speed [3]), and $c_2 = 6.65$ km/s [23]. Only the positive half of the first mini-Brillouin zone is shown. The dispersion curve is divided into a series of minibranches. The propagation velocity $d\omega/dq$ is proportional to the slope of the curve. Also shown in Fig. 1 are the dispersion curves for bulk a-Si (dashed line) and Mo (dotted line). For a bulk material, the laser-deposited thermal stress field launches a bipolar strain pulse [4] propagating with the bulk longitudinal sound velocity $c = \frac{d\omega}{dq}\big|_{\omega=0} = \sqrt{C_{33}/\varrho}$. This pulse is composed of the normal modes on the bulk dispersion curve. In a superlattice, a similar strain pulse can also be generated [24–26]. It consists mainly of the normal modes on the lowest minibranch. They are collectively excited near the surface and propagate in the z direction with an effective velocity given by [25]:

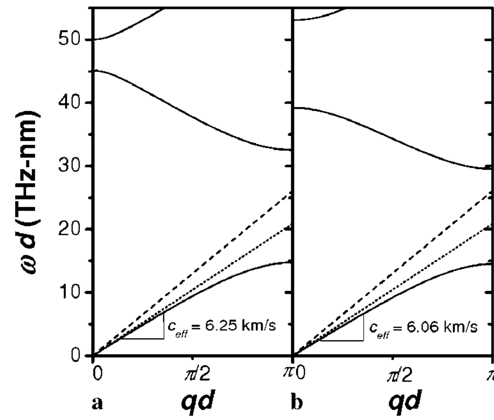

FIGURE 1 Calculated dispersion relation for longitudinal acoustic phonons in Si/Mo multilayers with **(a)** $\Gamma = 0.4$ and **(b)** $\Gamma = 0.6$. The dispersion curves for a-Si (*dashed*) and Mo (*dotted*) are also plotted for comparison

$$c_{\text{eff}} = \left.\frac{d\omega}{dq}\right|_{\omega=0} = \frac{d}{\sqrt{\frac{d_1^2}{c_1^2}+\frac{d_2^2}{c_2^2}+\left(\frac{Z_1}{Z_2}+\frac{Z_2}{Z_1}\right)\frac{d_1 d_2}{c_1 c_2}}} = \frac{1}{\sqrt{\frac{(1-\Gamma)^2}{c_1^2}+\frac{\Gamma^2}{c_2^2}+\left(\frac{c_1\varrho_1}{c_2\varrho_2}+\frac{c_2\varrho_2}{c_1\varrho_1}\right)\frac{\Gamma(1-\Gamma)}{c_1 c_2}}}\,. \tag{4}$$

In a perfectly periodic structure, this pulse propagates freely without being reflected or scattered at interfaces. It can be detected as it is partially reflected from the substrate and reenters the optically-sensitive surface region.

To extract the individual film velocities c_1 and c_2, one needs to have at least two sets of data from multilayers with different Γ ratios. The uncertainty in the densities ϱ_1 and ϱ_2 is a major source of error. From (4) the fractional error in c_{eff} due to the uncertainty in ϱ_i is

$$\frac{\Delta c_{\text{eff}}}{c_{\text{eff}}} = \frac{\Gamma(1-\Gamma)}{2}\frac{c_{\text{eff}}^2}{c_1 c_2}\left|\frac{Z_1}{Z_2}-\frac{Z_2}{Z_1}\right|\frac{\Delta\varrho_i}{\varrho_i}. \tag{5}$$

For Si/Mo multilayers, assuming $\Gamma = 0.5$ and bulk values for c_i and $Z_i(Z_2/Z_1 = 3.58)$, a 10% error in ϱ_i results in only 2.8% error in c_{eff}. For multilayers with smaller acoustic impedance mismatch, this error can be much less. In a similar way, we can assess the effect of uncertainty in Γ. For the same parameters, a 10% error in Γ results in only 1% error in c_{eff}.

3 Experimental

For our sound velocity measurements, we prepared five Si/Mo multilayer samples with $d \cong 7$ nm and various Γ ratios: 0.3, 0.4, 0.5, 0.6, and 0.7. For all samples the total number of periods is 40. Si/Mo mulilayers are important reflective coatings for extreme ultraviolet (EUV) projection lithog-

raphy [27, 28], and samples of superior and well-characterized qualities are available. Our samples were deposited on Si <100> substrates using an ultraclean ion beam sputtering (IBS) system, which is known for its ability to produce ultralow defect-density masks for EUV lithography [29]. Details of the IBS system were described in [29]. A focused beam of Ar ions was directed toward the Si or Mo targets, which were mounted back-to-back on a rotary stage. During multilayer deposition the stage was rotated from target to target. The substrates were spun around their axis of symmetry to obtain better azimuthal uniformity. Deposition times for the 40-bilayer multilayers were of the order of 100 min. Transmission electron microscopy indicates that the Si layers are amorphous and the Mo layers are polycrystalline [30].

Table 1 lists the values of Γ, d, peak EUV reflectance, and the centroid wavelength of the EUV reflectivity curve [31] for the five samples. The values of Γ were determined from the deposition times and the carefully calibrated deposition rates for the two constituents. The coating period d can be measured either by grazing incidence X-ray diffraction or by the centroid wavelength of the EUV reflectivity curves [31]. Both can provide an accuracy better than $\pm 0.1\%$. The EUV reflectometry measurements were performed at the Advanced Light Source (ALS) synchrotron facility at Lawrence Berkeley National Laboratory (LBNL). The reflectance spectrum for the sample with $\Gamma = 0.4$ is displayed in Fig. 2. The peak EUV reflectance (at 6° off normal) reaches 66.0% at a wavelength of 13.45 nm.

The acoustic pulses are impulsively excited in multilayers by optical absorption of an ultrashort "pump" light pulse (energy ~ 0.3 nJ), and detected as a reflectivity change of an attenuated (~ 0.03 nJ), time-delayed "probe" pulse. These light pulses were generated by a mode-locked Ti:sapphire laser operating at 800 nm wavelength, with a FWHM pulse duration of 130 fs and a repetition rate of 100 MHz. The pulses were focused onto an area of the sample in concentric spots with diameters of approximately 10 μm and 6 μm for pump and probe beams, respectively. The optical absorption occurs predominantly in Mo layers, with an effective penetration depth of ~ 400 Å. The optical energy is first absorbed by electrons in Mo and then, within a time of ~ 1 ps [32–34], transferred to the lattice via electron-phonon interaction. The stress field set up by this lattice heat then launches an acoustic pulse in the superlattice structure. A slight change ($\sim 10^{-5}$) of the optical reflectivity $\Delta R(t)$ is induced by these strain waves through the photoelastic effect.

Figure 3 displays an example of the measured $\Delta R(t)$ trace for the Si/Mo multilayer with $\Gamma = 0.4$. The acoustic echo emerges as a small bump on the ΔR curve at $t = 91.0 \pm 0.5$ ps (indicated with an arrow). This photoelastic signal is superimposed on a smoothly decaying photothermal background, which arises from the transient temperature rise and subsequent cooling in the films. The inset shows more clearly the acoustic echo after subtracting out the photothermal background. The shape and width of the echo are very similar to those in a pure Mo film [35], without obvious distortion or broadening. The ΔR signal amplitude of the echo is also comparable to that in the Mo sample with a similar total thickness and the same substrate. This indicates a good coating uniformity, without defects or deviation from periodicity, as well as good material and interface quality with very low acoustic attenuation and scattering. Figure 4 shows the Fourier transform

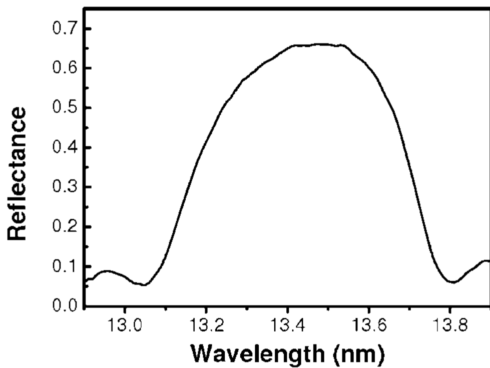

FIGURE 2 The EUV reflectance spectrum for the Si/Mo sample with $\Gamma = 0.4$

Γ	d (Å)	Peak EUV Reflectance	Centroid EUV Wavelength (Å)
0.3	68.5	61.2%	134.1
0.4	69.1	66.0%	134.4
0.5	69.5	64.7%	134.4
0.6	70.2	59.5%	134.7
0.7	70.6	50.0%	134.2

TABLE 1 Measured values of Γ, d, peak EUV reflectance and the centroid EUV wavelength for the five Si/Mo samples

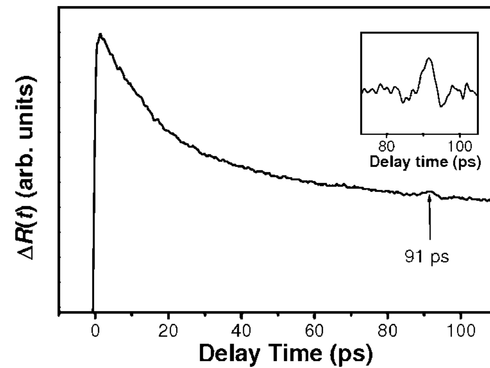

FIGURE 3 The measured $\Delta R(t)$ for the Si/Mo multilayer with $\Gamma = 0.4$. The acoustic echo is indicated with an *arrow*. The *inset* shows the magnified echo signal after subtracting out the photothermal background

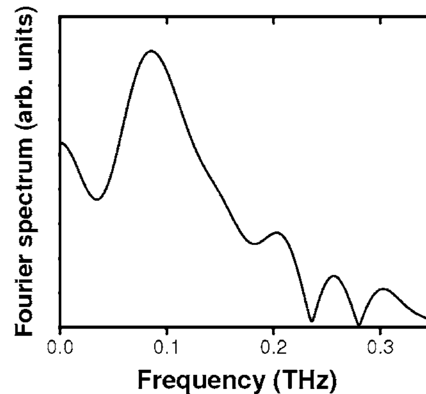

FIGURE 4 The Fourier transform spectrum for the acoustic echo

of the echo. It exhibits a very broad acoustic spectrum with a peak at around 90 GHz, and high-frequency components extending up to ∼ 200 GHz. These frequencies are significantly higher than the maximum frequency in conventional ultrasonic techniques.

4 Extraction of the individual sound velocities

The echo times τ and the effective longitudinal sound velocities c_{eff} for the five samples with various thickness ratios are displayed in Fig. 5a and b, respectively. The dashed curve in Fig. 5b is the theoretical prediction assuming the bulk values of longitudinal sound velocities in a-Si and Mo. It is slightly higher than the measured values. To extract the individual velocities in the a-Si and Mo layers, we use (4) to fit the experimental data, with c_1 and c_2 as the fitting parameters. ϱ_1 and ϱ_2 are assumed to be bulk densities. The parameters c_1 and c_2 obtained by least-square fitting (see the dotted curve in Fig. 5b) are 8.16 and 6.25 km/s. These values correspond to 98% and 94% of the bulk longitudinal velocities in a-Si and Mo, respectively. The estimated errors in c_1 and c_2 due to the uncertainty in Γ, ϱ_1, ϱ_2, and τ are about ±4%.

Several researchers have reported measured sound velocities for a-Si [1–3, 36] films prepared by various means, and the values range from 4.4 to 8.4 km/s. According to [3], the sound velocity in a-Si strongly depends on the method of film preparation. It was concluded that the sound velocity decreases following the preparation sequence of glow discharge (∼ 8.4 km/s [36]), ion implantation (∼ 7.5 km/s [1]), evaporation (∼ 6.3 km/s [3]), and sputtering (∼ 4.4 km/s [2]). This sequence indicates increasing void content in the deposited films. Our measured velocity, however, does not follow this expected trend. It is drastically different from those of the sputtered a-Si films studied previously [2], and is instead close to those of the films prepared by glow discharge [36].

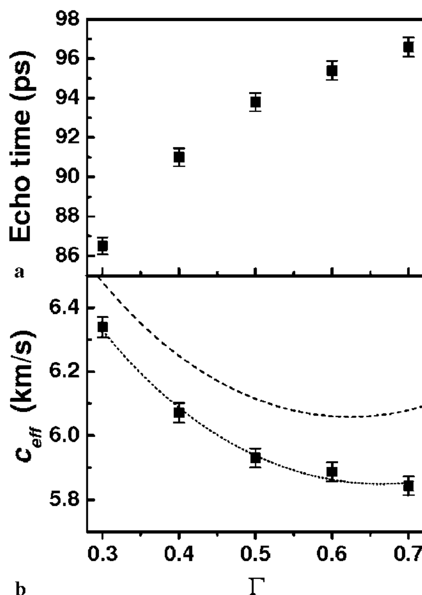

FIGURE 5 **(a)** The measured echo times τ vs. Γ. **(b)** The effective longitudinal sound velocities c_{eff} calculated from τ (*filled squares*); the *dotted curve* is a least-square fit to the data using (4); the *dashed curve* is the theoretical prediction assuming the bulk values of c_1 and c_2

To check if ion beam sputtering produces films with properties different from other sputtering techniques, we performed the same velocity measurement on another Si/Mo multilayer grown with DC magnetron sputtering for comparison. The Γ ratio of this sample is 0.5, and the measured c_{eff} is 5.7 km/s, which is similar to that of the corresponding ion-beam sputtered sample. We thus conclude that there is not much difference in the acoustic properties of a-Si films prepared by different sputtering techniques.

A possible explanation for the extraordinarily high sound velocity in our sputtered a-Si films, as compared to the previous results, is material densification due to contraction during multilayer deposition. It was found that there is a period contraction (∼ 0.7 nm) in Si/Mo multilayers. This results in a change in the elastic stiffness, and thus modifies the sound velocity. This contraction is correlated with the well-known fact that Si/Mo multilayers develop large compressive stress during growth, typically −450 to −350 MPa, which causes distortion of the extremely precise EUV optics [37–39].

5 Summary

We have demonstrated pulse-echo measurement of the longitudinal sound velocity in thin films of nanometer thickness using laser-based picosecond ultrasonics. By measuring the effective velocities of several Si/Mo multilayers with different thickness ratios, we can extract the individual velocities for a-Si and Mo films. Longitudinal sound velocities in ion-beam sputtered a-Si and Mo films of 2 to 5 nm thickness have been determined to be 98 and 94% of the bulk speed, respectively. Compared to the measured velocity for sputtered a-Si films in the literature, our study gives a significantly higher value. This is possibly caused by film contraction during deposition. We believe this technique is a useful tool for investigating the sound velocity of bulk acoustic waves in nanofilms.

ACKNOWLEDGEMENTS The authors would like to thank P.A. Kearney for preparing the Si/Mo multilayers. This work was supported in part by the national science council of Taiwan under grant No. NSC 93-2112-M-014-002 and NSC 93-2215-E-014-003.

REFERENCES

1 S.I. Tan, B.S. Berry, B.L. Crowder, Appl. Phys. Lett. **20**, 88 (1972)
2 L.R. Testardi, J.J. Hauser, Solid State Commun. **21**, 1039 (1977)
3 I.R. Cox-Smith, H.C. Liang, R.O. Dillon, J. Vac. Sci. Technol. A **3**, 674 (1985)
4 C. Thomsen, H.T. Grahn, H.J. Maris, J. Tauc, Phys. Rev. B **34**, 4129 (1986)
5 C. Thomsen, H.T. Grahn, H.J. Maris, J. Tauc, Opt. Commun. **60**, 55 (1986)
6 H.T. Grahn, D.A. Young, H.J. Maris, J. Tauc, J.M. Hong, T.P. Smith III, Appl. Phys. Lett. **53**, 2023 (1988)
7 H.T. Grahn, H.J. Maris, J. Tauc, K.S. Hatton, Appl. Phys. Lett. **53**, 2281 (1988)
8 T.C. Zhu, H.J. Maris, J. Tauc, Phys. Rev. B **44**, 4281 (1991)
9 H.N. Lin, R.J. Stoner, H.J. Maris, J.M.E. Harper, C. Cabral, J.M. Halbout, G.W. Rubloff, Appl. Phys. Lett. **61**, 2700 (1992)
10 Y.C. Lee, K.C. Bretz, F.W. Wise, W. Sachse, Appl. Phys. Lett. **69**, 1692 (1996)
11 G. Tas, J.J. Loomis, H.J. Maris, A.A. Bailes, J. Tauc, Appl. Phys. Lett. **72**, 2235 (1998)
12 D.M. Profunser, J. Vollmann, J. Dual, Ultrasonics **42**, 641 (2004)
13 S.M. Rytov, Akust. Zh. **2**, 71 (1956) [Sov. Phys. – Acous. **2**, 68 (1956)]

14 A. Kueny, M. Grimsditch, K. Miyano, I. Banerjee, C.M. Falco, I.K. Schuller, Phys. Rev. Lett. **48**, 166 (1982)
15 M.R. Khan, C.S.L. Chun, G.P. Felcher, M. Grimsditch, A. Kueny, C.M. Falco, I.K. Schuller, Phys. Rev. B **27**, 7186 (1983)
16 R. Danner, R.P. Huebener, C.S.L. Chun, M. Grimsditch, I.K. Schuller, Phys. Rev. B **33**, 3696 (1986)
17 P. Bisanti, M.B. Brodsky, G.P. Felcher, M. Grimsditch, L.R. Sill, Phys. Rev. B **35**, 7813 (1987)
18 A. Kueny, M. Grimsditch, B.Y. Jin, J.B. Ketterson, J.E. Hilliard, J. Appl. Phys. **56**, 1550 (1984)
19 C. Colvard, R. Merlin, M.V. Klein, A.C. Gossard, Phys. Rev. Lett. **45**, 298 (1980)
20 B. Jusserand, M. Cardona, in: *Light Scattering in Solids V: Superlattices and Other Microstructures,* ed. by M. Cardona, G. Guntherodt, Topics in Applied Physics Vol. 66 (Springer-Verlag, Berlin 1989)
21 E.C. Freeman, W. Paul, Phys. Rev. B **20**, 716 (1979)
22 C. Kittel, in *Introduction to Solid State Physics, 7th ed.* (Wiley, NY 1996)
23 *Landolt-Bornstein Numerical Data and Functional Relationships in Science and Technology*, *New Series*, ***II/5***, ed. by K.H. Hellwege, A.M. Hellwege (Springer-Verlag, Berlin, Heidelberg 1967)
24 W. Chen, Y. Lu, H.J. Maris, G. Xiao, Phys. Rev. B **50**, 14 506 (1994)
25 B. Bonello, B. Perrin, E. Romatet, J.C. Jeannet, Ultrasonics **35**, 223 (1997)
26 B.M. Clemens, G.L. Eesley, Phys. Rev. Lett. **61**, 2356 (1988)
27 C. Montcalm, S. Bajt, P.B. Mirkarimi, E. Spiller, F.J. Weber, J.A. Folta, Proc. SPIE **3331**, 42 (1998)
28 J.A. Folta, S. Bajt, T.W. Barbee, R.F. Grabner, P.B. Mirkarimi, T. Nguyen, M.A. Schmidt, E. Spiller, C.C. Walton, M. Wedowski, C. Montcalm, Proc. SPIE **3676**, 702 (1999)
29 P.A. Kearney, C.E. Moore, S.I. Tan, S.P. Vernon, R.A. Levesque, J. Vac. Sci. Technol. B **15**, 2452 (1997)
30 R.S. Rosen, D.G. Stearns, M.A. Viliardos, M.E. Kassner, S.P. Vernon, Y. Cheng, Appl. Opt. **32**, 6975 (1993)
31 E. Spiller, S.L. Baker, P.B. Mirkarimi, V. Sperry, E.M. Gullikson, D.G. Stearns, Appl. Opt. **42**, 4049 (2003)
32 S.I. Anisimov, B.L. Kapeliovich, T.L. Perelman, Zh. Eksp. Teor. Fiz. **66**, 776 (1974) [Sov. Phys. JETP, **39**, 375 (1975)]
33 J.G. Fujimoto, J.M. Liu, E.P. Ippen, N. Bloembergen, Phys. Rev. Lett. **53**, 1837 (1984)
34 R.W. Schoenlein, W.Z. Lin, J.G. Fujimoto, G.L. Eesley, Phys. Rev. Lett. **58**, 1680 (1987)
35 O.B. Wright, K. Kawashima, Phys. Rev. Lett. **69**, 1668 (1992)
36 M. Grimsditch, W. Senn, G. Winterling, Solid State Commun. **26**, 229 (1978)
37 P.A. Spence, M.P. Kanouff, A.K. Ray-Chaudhuri, Proc. SPIE **3676**, 724 (1999)
38 D.G. Stearns, R.S. Rosen, S.P. Vernon, Appl. Opt. **32**, 6952 (1993)
39 J.M. Freitag, B.M. Clemens, Appl. Phys. Lett. **73**, 43 (1998)